Int. J. Multiphase Flow Vol. 15, No. 3, pp. 403–419, 1989
Printed in Great Britain.

0301-9322/89 $3.00 + 0.00

PREDICTION OF THE CIRCUMFERENTIAL DISTRIBUTION OF FILM THICKNESS IN HORIZONTAL AND NEAR-HORIZONTAL GAS–LIQUID ANNULAR FLOWS

T. FUKANO
Faculty of Engineering, Kyushu University 36, 6-10-1 Hakozaki, Higashi-ku, Fukuoka, 812 Japan

A. OUSAKA
Technical College of the University of Tokushima, 2-1 Minamijosanjima, Tokushima, 770 Japan

(*Received* 1 *October* 1988; *in revised form* 7 *December* 1988)

Abstract—A theoretical model for predicting the circumferential film thickness distribution in horizontal and near-horizontal annular two-phase flows is presented. It is based upon a disturbance wave flow model which consists of disturbance waves and a base film. It differs from Laurinat's and Lin's models in that liquid is transferred in the circumferential direction by the pumping action of disturbance waves, which counteracts the drainage due to gravity, and that the effects of the induced secondary flow in the gas flow and the surface tension force have minor effects on the formation of the liquid film near the top of the tube cross section. The film thickness distribution predicted by the present model agrees with the experimental data much better than those predicted by Laurinat's model.

Key Words: two-phase flow, gas–liquid annular flow, horizontal pipe, inclined pipe, film thickness distribution, disturbance wave, pumping action, theory

1. INTRODUCTION

In recent theoretical researches into the circumferential distribution of the liquid film thickness of a gas–liquid two-phase annular flow in a horizontal pipeline, the discussion has focused on which is the main parameter controlling the film thickness distribution. Butterworth (1973) proposed the following four mechanisms:

(1) Spreading of the film by a wave action.
(2) Transfer of liquid by entrainment and deposition of droplets.
(3) Spreading by circumferential shear forces due to secondary gas flow.
(4) Spreading by surface tension forces.

Laurinat *et al.* (1985) and Lin *et al.* (1985) investigated this problem theoretically, based on their proposed flow models, taking all these mechanisms except the last one (4) into consideration. Their theoretical models, between which there are few differences, seem to be the best of those proposed previously. The present authors examined Laurinat's model in detail; i.e. circumferential film thickness distributions obtained theoretically using a computer code designed by the present authors, following Laurinat's theoretical model exactly, were compared with the experimental data measured by the present authors. The results show that: (a) the difference in the film thickness between the theory and the experimental data becomes extremely large, and there were cases where even the computer code did not work if the volumetric flux of the liquid, j_L, exceeded 0.06 m/s; and (b) the secondary flow of the gas phase, mechanism (3), is the most important factor to affect the liquid film distribution in a horizontal annular two-phase flow, or to transfer liquid towards the top of the tube against the drainage due to gravity.

Although a direct and quantitative examination into the role of the secondary gas flow cannot be made as yet, because the experimental data on it obtained in an actual gas–liquid two-phase flow have not been reported, the results seem to overvalue the role of the secondary gas flow. According to the present authors' extensive experimental data (Sekoguchi *et al.* 1982; Fukano *et al.* 1985), disturbance waves are almost always generated near the bottom (even under the low liquid

flow rate condition) and the disturbance waves play an important role in maintaining a liquid film near the top of the tube.

To calculate the circumferential film thickness distribution, in this paper a new flow model is proposed in which the liquid film is assumed to consist of disturbance waves and the base film. The emphasis is on the wave action, which was concluded to be negligible in Laurinat's model, and the role of the secondary gas flow is neglected in the model proposed here for estimating the forces required to transfer liquid towards the top of the tube. In this paper the film thickness distributions calculated by this new model are compared with the experimental data of horizontal and near-horizontal pipelines (Sekoguchi *et al.* 1982; Fukano *et al.* 1983; Fukano & Ousaka 1987) and the mechanism for spreading the liquid film near the top of the tube is discussed.

2. EXPERIMENT

2.1. Experimental apparatus and conditions

Figure 1 shows a schematic diagram of the experimental apparatus. The test section was a smooth tube of 26.0 mm i.d. and total length 6.7 m made of transparent acrylic resin to observe the flow pattern. The inclination angles of the test section are $-10°$ (downflow), $0°$ (horizontal flow), $10°$ and $15°$ (upflow). Film thickness was measured at about 3.7 m ($142D$) downstream of the air–water merging section by the needle contact method, shown in figure 2.

The device for the needle contact method consists of a pair of electrodes: one is a point electrode at the tip of an electrically shielded needle, which can be traversed both radially and circumferentially; the other is a fixed electrode mounted flush with the inner surface. The needle is made of a platinum wire of 0.2 mm dia and the fixed electrode is made of a brass bar of 5 mm dia. Direct current with a constant voltage is supplied to the two electrodes as shown in figure 2, and the current variation, due to the difference in the resistances of air and water, is converted into a voltage variation via a load resistance. The output signal takes a maximum or a minimum value according to whether the needle is in contact with the liquid film or the gas phase. The shape of the output signal (displayed on an oscillograph), however, is not always square but triangular, especially when the needle is in contact with one phase for a very short time because there is a time lag in the response of the measuring system which includes the deformation effect of the gas–liquid interface. Consequently, the time ratio of the existence of the liquid phase takes different values according

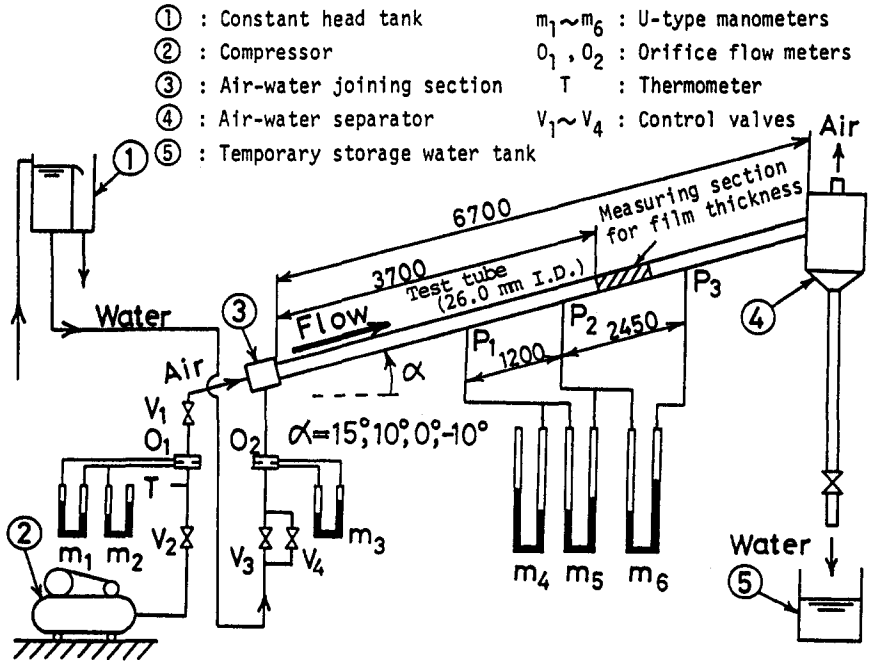

Figure 1. Schematic diagram of the test apparatus.

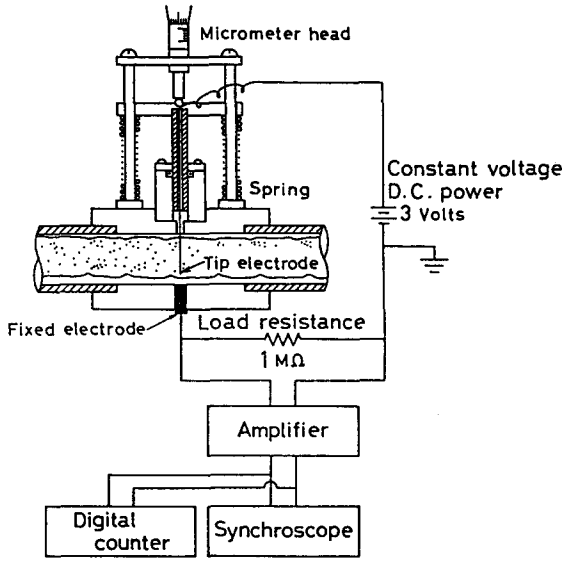

Figure 2. Resistivity needle contact method.

to which level we adopt between the maximum and the minimum value of the output signal under analysis. In this research the level, called the slice level (Sekoguchi *et al.* 1975), is set at 35% of the maximum amplitude measured from the maximum output voltage which shows the existence of the water phase. The circumferential measurements are made at seven locations; i.e. every 30° from the top to the bottom of the tube. Measuring positions along the radius are selected according to the flow configuration.

The experimental conditions are as follows: working fluids, air and water; static pressure, 0.102–0.135 MPa; water temperature, ~20°C; ranges of the volumetric flux and superficial Reynolds number of air, $j_G = 10$–50 m/s, $Re_{SG} = 1.77 \times 10^4$–$1.01 \times 10^5$; and those of water, $j_L = 0.006$–0.40 m/s, $Re_{SL} = 18$–1.04×10^4. The flow pattern observed is mainly annular flow, containing also froth and separated flows near the annular flow.

2.2. *Experimental results*

Figures 3(a–f) show typical examples of the experimental data for the circumferential distributions of film thickness, $(t_{fm})_\theta$, which is defined by the following equation:

$$(t_{fm})_\theta = R - \sqrt{R^2 - 2\int_0^R (\eta)_\theta r \, dr}, \qquad [1]$$

where R is the radius of the tube, η is the time ratio of the existing liquid phase measured by the needle contact method and θ is the circumferential position expressed by the sector angle from the top of the tube cross section. The coordinate axis in the radial direction is the film thickness and the inclination angle of the test section is the parameter; □—·····—□ shows $\alpha = 15°$, △—·—△ shows $\alpha = 10°$, ○——○ shows $\alpha = 0°$ and ▲····▲ shows $\alpha = -10°$; S_p, F, A_D and A_F express the flow patterns observed, S_p for separated flow, F for froth flow, A_D for disturbance-wave-dominated annular flow and A_F for froth-flow-like annular flow.

As clearly shown in figures 3(a–f), the distribution becomes uniform as the gas flow rate j_G increases, signifying that the larger the gas flow rate, the stronger the effect of the interfacial shear stress on the liquid film flow, while the gravitational force is a controlling factor in the low gas flow rate region.

3. THEORY

3.1. *Flow model; pumping action of disturbance waves*

A disturbance wave flow model is introduced to define the parameters R_A^+, R_D^+, $\tau_{YZ}^+|_{h^+}$, $\tau_{YX}^+|_{h^+}$, τ_{XX}^+ and τ_{XZ}^+, shown in figure 5 and included in the basic equations as the coefficients. As shown

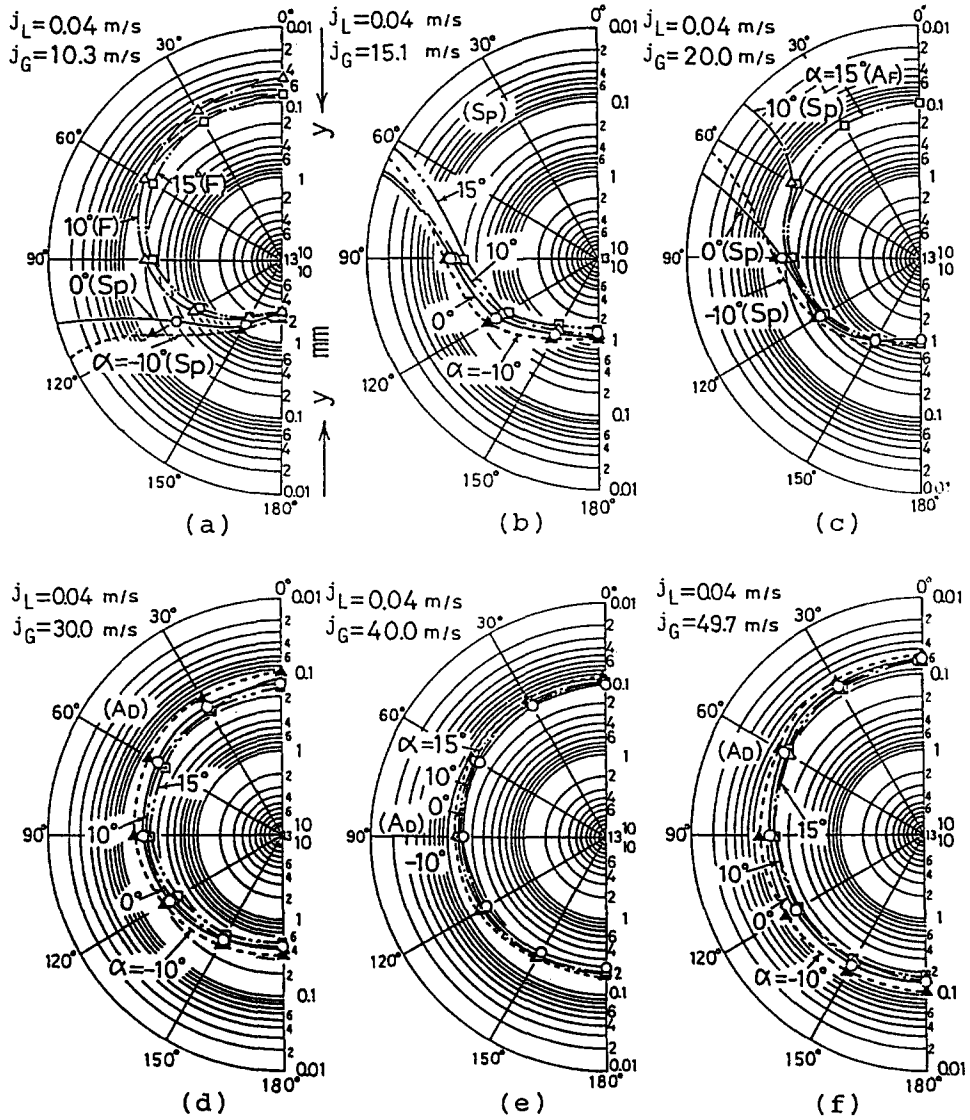

Figure 3. Circumferential distribution of the film thickness (experiment).

in figure 4, the liquid film is assumed to consist of disturbance waves and the base film. The disturbance waves are propagated in the axial direction by the pressure difference between the rear and the front of the disturbance wave.

The height of the disturbance wave is greater near the bottom of the pipe and smaller near the top, as shown in figure 4 which is drawn from a relative frame of reference fixed to disturbance waves with the velocity of C_D. The crest of the disturbance wave juts into the gas flow with a higher

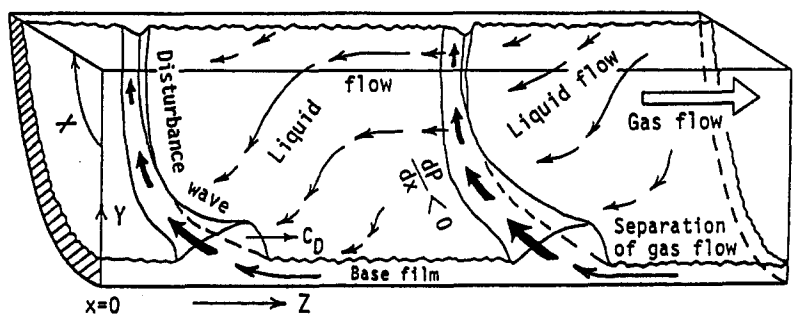

Figure 4. Flow model: pumping action of the disturbance wave.

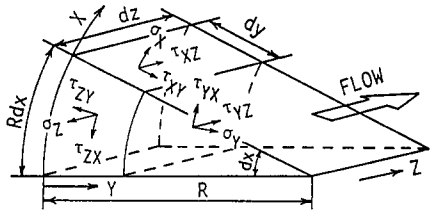

Figure 5. Coordinate axes and nomenclature.

velocity at the bottom of the tube than at the top. On the other hand, the gas flow separates in the region just in front of the disturbance waves where the static pressure may be assumed to be constant. Therefore, the static pressure rise caused by the stagnation of the gas flow behind the disturbance wave is larger at the bottom and decreases towards the top. That is, a negative pressure gradient is generated along the disturbance wave from the bottom to the top. Because the liquid film is thin, the static pressure or the normal stress σ_x in the liquid film can be assumed uniform. Due to this normal stress gradient the liquid included in the disturbance wave is pumped up towards the top, this is called the pumping action of disturbance waves in this paper. At the same time, part of the pumped up liquid is being discharged continuously behind the disturbance wave and forms the base film. As a result, the disturbance wave gradually reduces in scale towards the top of the pipe. Liquid in the base film drains into the bottom and is reabsorbed into the next disturbance wave. Due to the static pressure gradient, the secondary gas flow is also generated. The effect of the secondary flow on the liquid flow in the circumferential direction is, however, neglected, as described in the introduction.

Viewed from the relative frame of reference the liquid flow is steady (shown by arrows in figure 4). From a fixed frame of reference, however, this phenomenon is unsteady, i.e. an amount of liquid is moved towards the top when a disturbance wave passes by a certain cross section of the pipe, and drains to the bottom as a liquid film after the disturbance wave has passed. This process is repeated every time a disturbance wave passes. It must be noted that this mechanism of spreading liquid towards the top of the pipe is another explanation of the wave spreading model.

It is widely known that the disturbance waves pass intermittently. Then the present model is, strictly speaking, fundamentally based on an unsteady flow. Actually, however, the interval between successive disturbance waves is considered to be sufficiently short compared with the time taken for liquid to flow down from near the top of the tube to the bottom as a thin liquid film. This means that the unsteady flow in question can be approximated by a steady flow. Therefore, it is assumed in this paper that the pumping action of the disturbance wave continues steadily and the force required to move the liquid towards the top of the pipe is regarded as the normal stress when considering the drainage of the liquid.

3.2. Assumptions

Figure 5 shows the coordinate axes and the nomenclature used in the analysis, X being for the circumferential direction, Y for the radial direction, Z for the axial direction, σ for the normal stress and τ for the shear stress. The gas phase flows in a core region of the circular tube and the liquid flows on the tube inner surface as a liquid film as well as in the core region as small droplets. The assumptions made in the analysis of the film are:

(1) The liquid flow in the film is fully developed, i.e. it does not change with time nor in the axial direction.
(2) The film is thin compared with the diameter of the tube.
(3) The velocity of the liquid in the film in the axial direction is much higher than that in the circumferential direction.
(4) The eddy viscosity in the liquid film is isotropic and governed by the axial flow of the liquid.
(5) The distribution of the eddy viscosity is the same as that for single-phase flow in a tube, i.e. the velocity profiles proposed by Von Karman are used for determining the eddy viscosity.

3.3. Basic equations

As shown in figure 5, the volume element with the sides of length of $R\,dx$, dy and dz is considered as a control volume; u, v and w are the velocity components in the X, Y and Z directions, respectively, p is the static pressure and g is the gravitational acceleration.

By taking the assumptions described in section 3.2 into consideration and using the continuity equation for the liquid flow, [2], the simplified and nondimensionalized continuity and momentum equations are expressed as follows:

$$\frac{\partial u^+}{R^+ \partial x^+} + \frac{\partial v^+}{\partial y^+} = 0, \qquad [2]$$

$$\frac{\partial \tau_{YZ}^+}{\partial y^+} + \frac{\partial \tau_{XZ}^+}{R^+ \partial x} \mp \nu_L g \sin\alpha \sqrt{\left(\frac{\rho_L}{\tau_s}\right)^3} = 0 \qquad [3]$$

and

$$\frac{\partial \tau_{YX}^+}{\partial y^+} + \frac{\partial \tau_{XX}^+}{R^+ \partial x} - \frac{\sin x \cdot \cos\alpha}{R^+ \mathrm{Fr}} - \frac{\cos x}{R^{+2}\mathrm{Fr}} \frac{dh^+}{dx} = 0, \qquad [4]$$

where the pressure terms are eliminated from the momentum equations in the directions of X and Y. The plus and minus signs are used to represent downflow and upflow, respectively. The velocities are nondimensionalized by the friction velocity V^*, the shear stresses by the wall shear stress in a gas single-phase flow τ_s, and the lengths by V^*/ν_L; ν_L is the kinematic viscosity.

Integrating [3] and [4] from $y = y^+$ to h^+, the following integral momentum equations are obtained (where h^+ is the nondimensionalized film thickness):

$$\tau_{YZ}^+|_{h^+} - \tau_{YZ}^+|_{y^+} + \frac{h^+ - y^+}{R^+} \frac{\partial \tau_{XZ}^+}{\partial x} \mp (h^+ - y^+)\nu_L g \sin\alpha \sqrt{\left(\frac{\rho_L}{\tau_s}\right)^3} = 0 \qquad [5]$$

and

$$\tau_{YX}^+|_{h^+} - \tau_{YX}^+|_{y^+} + \frac{h^+ - y^+}{R^+} \frac{\partial \tau_{XX}^+}{\partial x} - \frac{h^+ - y^+}{R^+ \mathrm{Fr}} \left(\sin x \cdot \cos\alpha + \frac{\cos x}{R^+} \frac{dh^+}{dx}\right) = 0. \qquad [6]$$

By assumption [5] the shear stresses τ_{YZ}^+ and τ_{YX}^+ are expressed using the dimensionless eddy diffusivity ϵ_{YZ}^+ as follows:

$$\tau_{YZ}^+ = (1 + \epsilon_{YZ}^+) \frac{\partial w^+}{\partial y^+} \qquad [7]$$

and

$$\tau_{YX}^+ = (1 + \epsilon_{YZ}^+) \frac{\partial u^+}{\partial y^+}. \qquad [8]$$

By substituting [7] and [8] into [5] and [6] and integrating them from $y^+ = 0$ to y^+, the following equations are obtained:

$$\int_0^{y^+} \frac{\tau_{YZ}^+|_{h^+}}{1 + \epsilon_{YZ}^+} dy^+ + \int_0^{y^+} \frac{h^+ - y^+}{R^+} \frac{\partial \tau_{XZ}^+}{\partial x} \frac{dy^+}{1 + \epsilon_{YZ}^+} \mp \int_0^{y^+} (h^+ - y^+)\nu_L g \sin\alpha \sqrt{\left(\frac{\rho_L}{\tau_s}\right)^3} \frac{dy^+}{1 + \epsilon_{YZ}^+} = w^+ \qquad [9]$$

and

$$\int_0^{y^+} \frac{\tau_{YX}^+|_{h^+}}{1 + \epsilon_{YZ}^+} dy^+ + \int_0^{y^+} \frac{h^+ - y^+}{R^+} \frac{\partial \tau_{XX}^+}{\partial x} \frac{dy^+}{1 + \epsilon_{YZ}^+} - \int_0^{y^+} \frac{h^+ - y^+}{R^+ \mathrm{Fr}} \left(\sin x \cdot \cos\alpha + \frac{\cos x}{R^+} \frac{dh^+}{dx}\right) \frac{dy^+}{1 + \epsilon_{YZ}^+} = u^+. \qquad [10]$$

The nondimensionalized flow rates per unit length in the direction of Z and X, Γ_Z^+ and Γ_X^+, are calculated by $\int_0^{h^+} w^+ \, dy^+$ and $\int_0^{h^+} u^+ \, dy^+$, respectively. So the following equations are obtained:

$$I_1 \tau_{YZ}^+|_{h^+} + \frac{I_2}{R^+}\frac{\partial \tau_{XZ}^+}{\partial x} \mp I_2 v_L g \sin\alpha \sqrt{\left(\frac{\rho_L}{\tau_s}\right)^3} = \Gamma_Z^+ = \bar{w}^+ h^+ \qquad [11]$$

and

$$I_1 \tau_{YX}^+|_{h^+} + \frac{I_2}{R^+}\frac{\partial \tau_{XX}^+}{\partial x} - \frac{I_2}{R^+ \mathrm{Fr}}\left(\sin x \cdot \cos\alpha + \frac{\cos x}{R^+}\frac{dh^+}{dx}\right) = \Gamma_X^+, \qquad [12]$$

where

$$I_1 = \int_0^{h^+}\int_0^{y^+} \frac{1}{1+\epsilon_{YZ}^+} dy_1^+ \, dy_2^+ \qquad [13]$$

and

$$I_2 = \int_0^{h^+}\int_0^{y^+} \frac{h^+ - y^+}{1+\epsilon_{YZ}^+} dy_1^+ \, dy_2^+. \qquad [14]$$

On the other hand, Γ_X^+ is related to the droplet deposition rate R_D^+ and the atomization rate R_A^+ by the following equation:

$$\frac{d\Gamma_X^+}{R^+ dx} = R_D^+ - R_A^+. \qquad [15]$$

These fundamental equations are similar to those used in the analyses by Laurinat *et al.* (1985) and Lin *et al.* (1985).

Γ_Z^+, Γ_X^+ and h^+ are solved by the simultaneous equations [11], [12] and [15] if all the unknown parameters in these equations can be defined, as will be described in the next section.

3.4. Definition of the parameters included in the basic equations

As described in the introduction the shear force acting on the gas–liquid interface in the circumferential direction due to the secondary gas flow $\tau_{YX}^+|_{h^+}$ is neglected. A simple examination certifies that $d\tau_{XZ}^+/dx$ is negligibly small, about 1% of the values of the other terms in the case $j_L = 0.01$ m/s and $j_G = 50$ m/s if it is calculated by the formula proposed by Laurinat *et al.*, for example. Neglecting this term divides the computational time in half without deteriorating the solution of the film thickness distribution.

3.4.1. τ_{XX}^+. Based on the flow model introduced in section 3.1 a nonuniform static pressure distribution is created inside the disturbance wave by the nonuniform distribution of the stagnation pressure along it, which causes a nonuniform distribution of the normal stress τ_{XX}^+ in the disturbance wave. We then assume that τ_{XX}^+ is linearly related to the static pressure gradient. It is difficult at present, however, to determine accurately the static pressure gradient. It is also assumed that the stagnation pressure just behind the disturbance wave is proportional to the pressure difference between the rear and the front of the disturbance wave, as shown in the following equation, with a proportional constant of C_1:

$$\tau_{XX} = -C_1 \frac{\Delta p}{\tau_s} = -C_1 \frac{\rho_G[(u_{G1} - C_D)^2 - (u_{G2} - C_D)^2]}{4\tau_s}, \qquad [16]$$

where ρ_G is the density of the gas, C_D is the disturbance wave velocity, u_{G1} and u_{G2} are the gas velocities at the tube cross sections far upstream and just ahead of the disturbance wave where the separation of the gas flow takes place, and they are determined by dividing j_G by the tube cross-sectional area minus the area occupied by the base film and the disturbance wave, respectively. By using the present authors' experimental data obtained for air–water annular

flow in a horizontal pipe of 26.0 mm i.d. for $j_G > 20$ m/s, they are correlated by the following equations:

$$u_{G1} = 0.224 + 91.8 j_L + 1.02 j_G, \quad [17]$$

$$u_{G2} = j_G \quad [18]$$

and

$$\frac{C_D}{j_L} = 0.344 \left(\frac{h}{R}\right)^{-1.244}, \quad [19]$$

where u_{G1}, u_{G2}, j_L and j_G are in m/s.

3.4.2. R_A^+. The atomization rate from the liquid film R_A^+ is determined by the correlation proposed by Whalley *et al.* (1974):

$$R_A^+ = \frac{52.24\, S^2}{\rho_L v^*}. \quad [20]$$

This relation was obtained by the force balance between the interfacial stress τ_i and the surface tension force. Here ρ_L is the density of liquid and

$$S = \frac{\tau_i h}{\sigma} \quad [21]$$

and

$$\tau_i = \frac{dp}{dz} \frac{R - h}{2}. \quad [22]$$

The judgment whether liquid is entrained or not will be discussed in section 3.5.

3.4.3. R_D^+. The deposition rate of the droplets R_D^+ is decided by the following equation:

$$R_D^+ = \frac{k_D C_E}{\rho_L v^*}, \quad [23]$$

where the concentration of the droplets, C_E(kg/m^3) is determined by the following equation, obtained by fitting Hutchinson & Whalley's (1973) data by the method of least squares:

$$\log_{10} C_E = 2.10 + 1.86 \log_{10} S, \quad [24]$$

where S is already defined in [21] and changes with the change in the film thickness, accordingly C_E changes circumferentially. The above take into consideration that the deposition must be greater at locations where the atomization rate is higher. k_D is a deposition coefficient determined by the following equation, which holds under a sufficiently developed flow condition:

$$k_D = \frac{\int_0^\pi R_A \, dx}{\int_0^\pi C_E \, dx}. \quad [25]$$

3.4.4. $\tau_{YZ}^+|_{h^+}$. The interfacial shear stress $\tau_{YZ}^+|_{h^+}$ is decided by the following correlation, which was obtained by Fukano *et al.* (1986) for a horizontal rectangular duct and can be applied for a disturbance wave flow:

$$\tau_{YZ}^+|_{h^+} = \frac{f_i}{f_{SG}} = 1.0 + 6.1 \times 10^{-5} (X^{0.8} \mathrm{Re}_{LF})^{0.65} \mathrm{Re}_{SG}^{0.7}, \quad [26]$$

where X is the Martinelli parameter, f_i is the interfacial friction factor and f_{SG} is the wall friction factor for a single-phase flow.

3.5. Criterion for the generation of entrained droplets

According to a criterion proposed by Woodmansee & Hanratty (1969), entrained droplets are generated if the flow condition satisfies the following inequality:

$$\mathrm{We} = \frac{\rho_G w_{rel}^2 \Delta h}{\sigma} > 5.5. \quad [27]$$

Taking the present flow model into consideration, the wave height of the disturbance wave h_D is used in place of the wave height Δh and the gas velocity relative to the disturbance wave, $u_{G1} - C_D$, replaces w_{rel}:

$$\left(\frac{h_D}{R}\right)_\theta = 10^{K0}\left(\frac{h}{R}\right)^{K1}, \quad [28]$$

where

$$K0 = 3.77 - 1.13\theta \quad [29]$$

and

$$K1 = 2.58 - 0.579\theta, \quad [30]$$

and where θ is the sector angle measured from the top of the tube and expressed in degrees.

3.6. Calculation

The flow chart used in solving the basic equations [11], [12] and [15] numerically is shown in figure 6. At this stage of the analysis of the present paper the film thickness at the bottom $(h)_{180}$, the distribution of the wave height of the disturbance wave $(h_D)_\theta$ and the pressure gradient dp/dz should be known parameters, as well as the flow conditions of both phases, j_G and j_L, and the properties of both phases. Once $(h)_{180}$ is given, the mean liquid velocity w^+ satisfying [11] is determined by the *regula falsi* method. Then Γ_z^+ is given as the product of h^+ and w^+. By using these parameters Γ_x is determined from the droplet exchange rate [15] with the boundary condition $(\Gamma_x)_{180} = 0$. Where the initial value of C_D is determined from [19] by assuming $\bar{h} = (h)_{180}$, then the decrease in the film thickness in the circumferential direction is calculated from dh^+/dx in [12], which decides the film thickness at the next position. This series of calculations is repeated up to the top of the tube, which is shown by loop ② in figure 6. If the difference between the newly

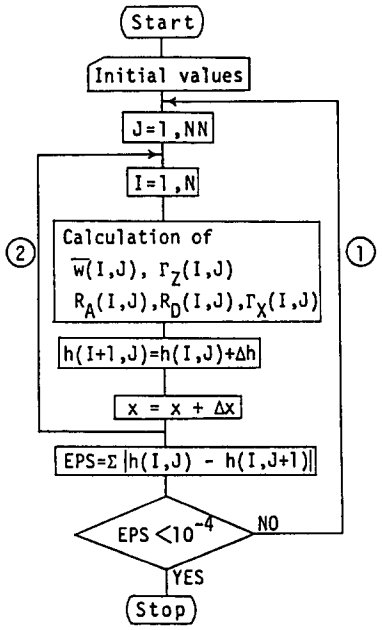

Figure 6. Flow chart of the calculation of the film thickness.

calculated circumferential distribution of the film thickness (determined by changing the value of C_1) and the previous one, which is shown by loop ① in figure 6, is within a predetermined error, it is considered to be a final solution.

It must be noted that Laurinat's model includes two parameters which must be determined by the iteration method, whereas the present model includes only one, C_1 in [16], and it is easy to determine.

4. RESULTS AND DISCUSSION

4.1. Comparison with the present experimental data

Figures 7(a–h) show examples of the comparison of the theoretical results with the experimental data. In these figures the broken and solid lines show the experimental and the numerical calculations, respectively. The coincidence between the solid and broken lines is good, signifying that the circumferential distribution of the film thickness can be predicted satisfactorily by the present method.

The film Reynolds number, Re_{LF}, shown in the figures is defined by using the total liquid flow rate, obtained theoretically by integrating circumferentially the local liquid flow rate. It is slightly smaller than the experimental value of the superficial liquid Reynolds number, Re_{SL}, which is defined by the volumetric flux of the liquid phase j_L, over the whole experimental range except for cases with large values of j_L. The difference between Re_{LF} and Re_{SL} becomes greater with increasing j_L.

There may be two reasons for this trend:

(1) Part of the total flow rate of the liquid, j_L, flows as entrained droplets and the entrainment increases with rising j_L (Ousaka *et al.* 1982).
(2) The distribution of eddy diffusivity, i.e. the velocity profile suitable for a single-phase flow is used for a liquid film flow. According to the experimental data obtained by the present authors (Fukano *et al.* 1987), the liquid particle velocity near the gas–liquid interface is much higher than that determined by assuming a linear velocity profile in the thin liquid film because the liquid particles near the interface can get extra flow energy from a high-speed gas flow, especially in cases where the gas volumetric flux exceeds ~40 m/s. This problem, however, requires further investigation.

In figures 7(e, g) the same comparisons are made for the case where a part of the tube surface is dried out near the top of the tube. Both distributions agree well with each other. The local film thickness at a location where the liquid film is dried out can be correlated by the following expression:

$$h_c = 23.1\, j_G^{-1.45}, \qquad [31]$$

where h_c is in mm and j_G is in m/s.

Figures 8(a–f) show similar comparisons for the cases with inclined test sections, $\alpha = -10°$, 10° and 15°. In these cases also the predicted values agree well with the experiments.

In the following the predicted distributions of the parameters relevant to the film thickness distribution will be discussed.

Figures 9(a–h) show examples of the predicted distributions of the droplet atomization rate R_A^+ and the deposition rate R_D^+. Both R_A^+ and R_D^+ increase towards the bottom ($\theta = 180°$) of the tube because the liquid film thickness h and, therefore, S and C_E increase towards the bottom. The curves for R_A^+ and R_D^+ intersect near $\theta = 90° - 120°$ for the case where the complete tube surface is covered with a liquid film. In the region below the point of intersection the atomization exceeds the deposition, while in the upper part of the tube the deposition is stronger. This tendency also holds good in the case where a dry surface exists near the top, although the two curves of R_A^+ and R_D^+ intersect at a larger sector angle θ.

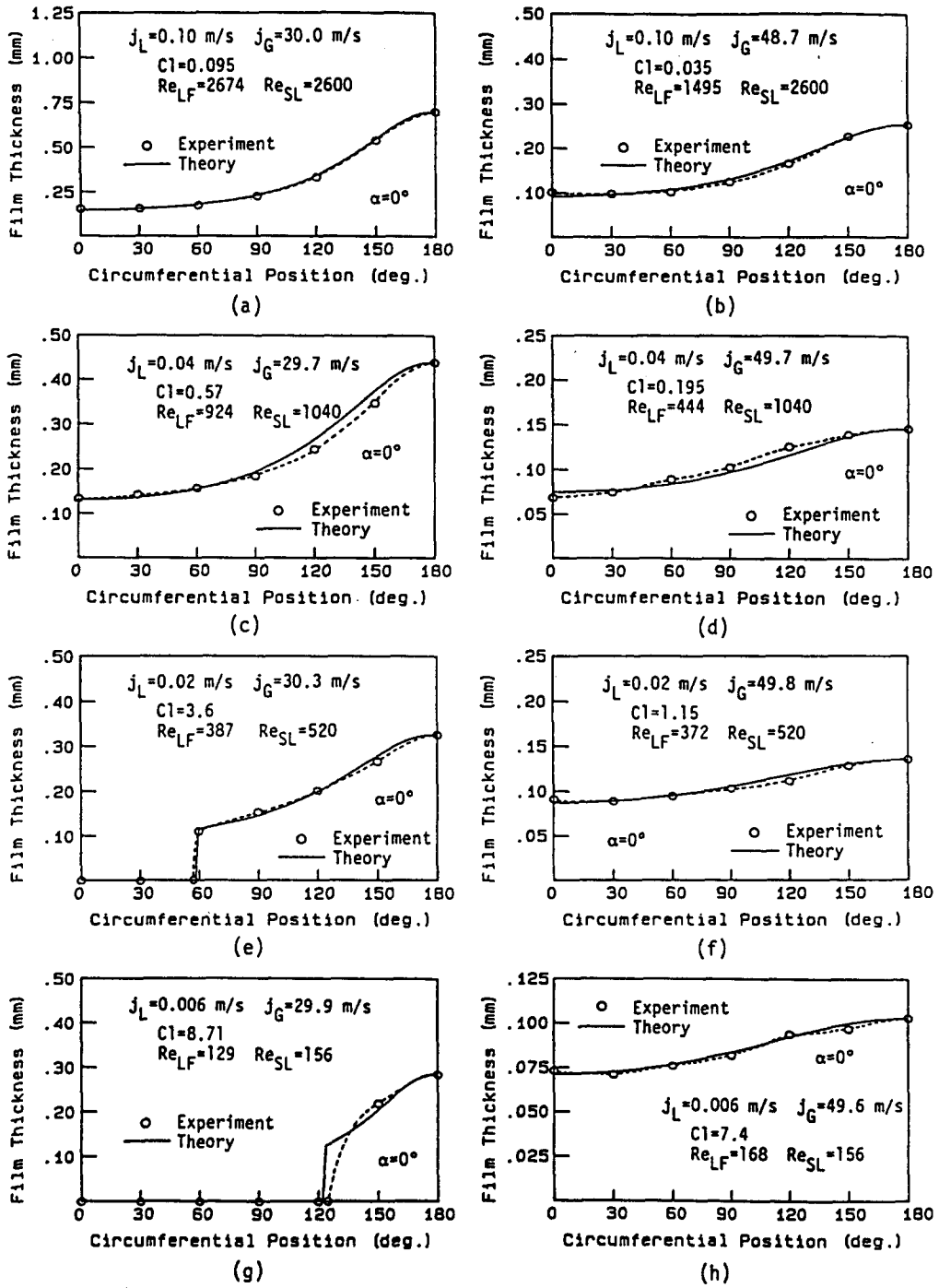

Figure 7. Comparison of the predicted film thickness distribution with the experimental data ($\alpha = 0°$).

Figures 10(a–h) show the relative magnitudes of the terms P2, P3 and P4 (which correspond to the second, third and fourth terms on the l.h.s. of [12], respectively) and that of the droplet exchange rate Γ_x (which is determined by these terms and the droplet deposition and atomization rates, R_D^+ and R_A^+). In this paper the first term on the l.h.s. of [12] is assumed to be zero.

As clearly shown in these figures, the term P2 is the main factor in coping with the drainage of the liquid due to gravity. That is, liquid is transferred by the pumping action of the disturbance wave, i.e. by the wave spreading towards the top, which results in the formation of a liquid film there. On the other hand, the roles of droplet deposition and atomization are very limited in the present experimental range.

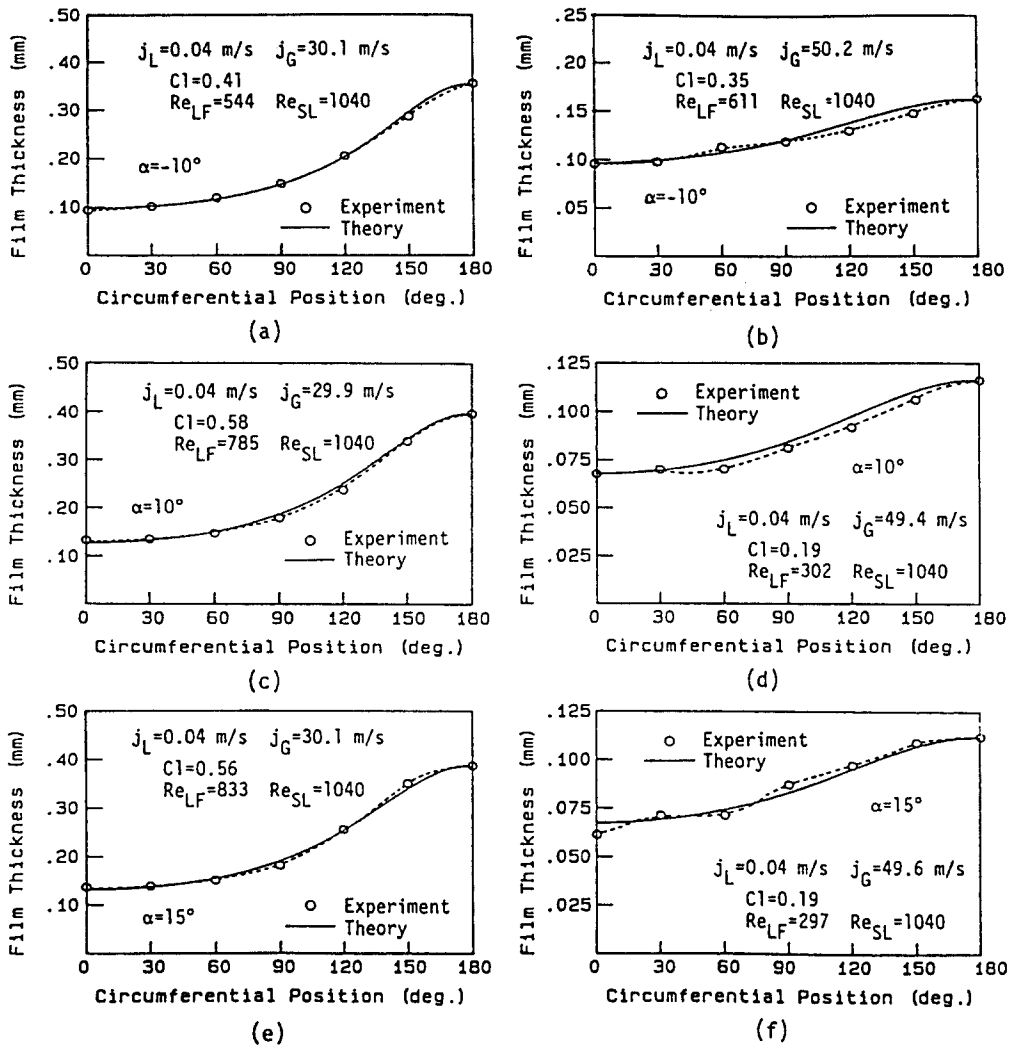

Figure 8. Comparison of the predicted film thickness distribution with the experimental data ($\alpha = -10°$, 10° and 15°).

4.2. Comparison with Laurinat's model

As already described in the introduction, Laurinat's model is the most sophisticated of those proposed previously to explain the circumferential distribution of the film thickness. Their model is based on a one-layer liquid film with an averaged constant film thickness. On the other hand, the present model is based on a disturbance wave flow model in which the disturbance wave has a pumping action to feed the liquid to the top of the tube. This pumping action is caused by the difference in the static pressure rise due to the stagnation of the gas flow just behind the disturbance wave. Another important difference between the two models is that there is only one unknown constant in the present model, the value of which is determined by iteration in the numerical calculation, whereas there are two in Laurinat's model, thereby being more difficult to determine and making the convergence of the numerical solution much slower.

Figures 11(a, b) show the results obtained with Laurinat's method. Comparison of these figures with figures 7(c, d) reveals that the predicted values agree with the experimental data with the same degree of accuracy as those obtained by the present method, although in a limited range of flow conditions. That is, the accuracy of the agreement in the case of Laurinat's method deteriorates as the liquid flow rate, j_L, increases. For example, the converged solution cannot be obtained under the condition where the liquid film breaks up near the top of the tube nor under the conditions $j_L > 0.06$ m/s and/or $j_G < 35$ m/s even if the whole tube surface is covered with a liquid film. In this

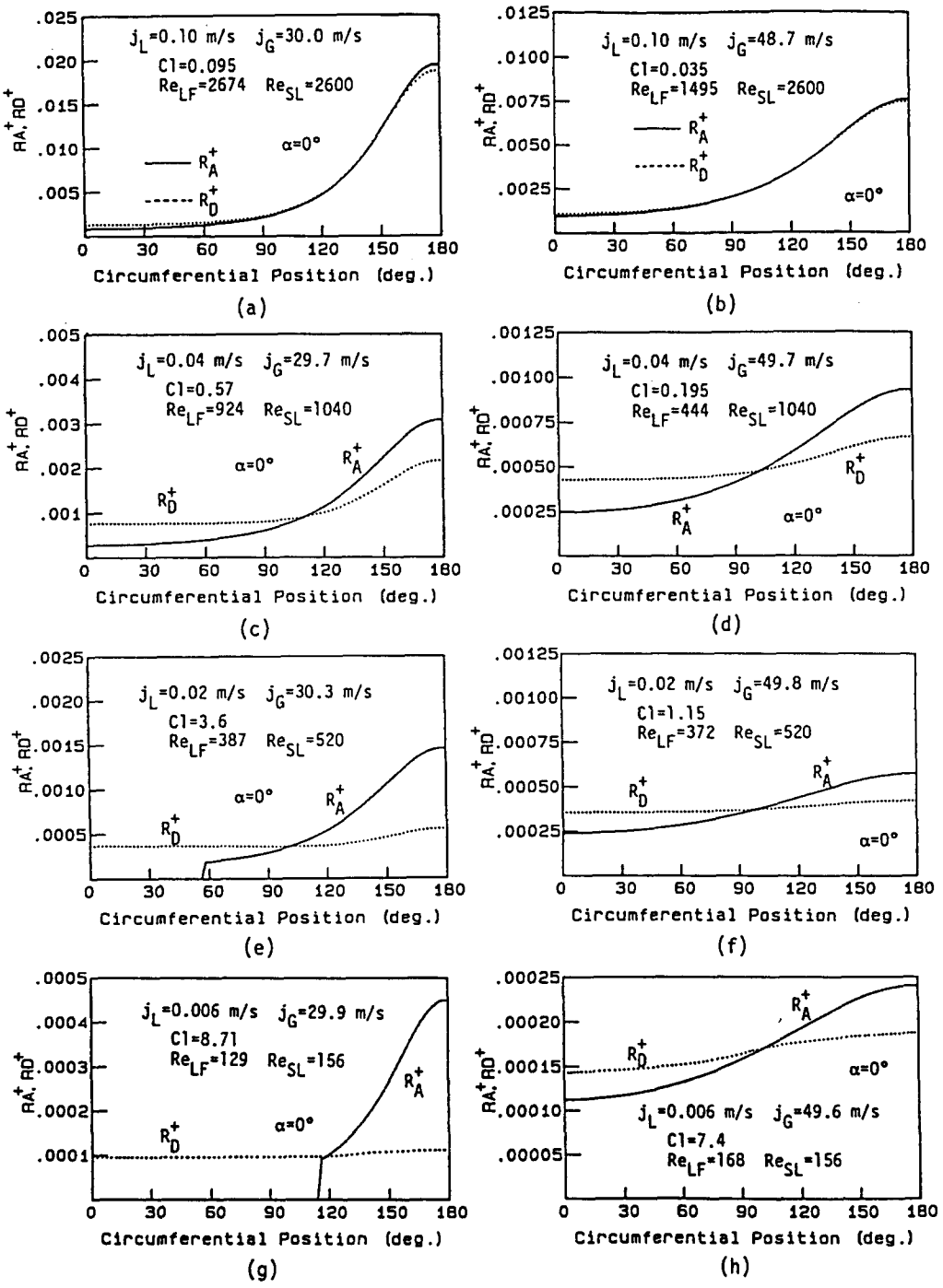

Figure 9. Distributions of the generation and deposition of entrainment predicted by the present method ($\alpha = 0°$).

respect also the present method has the advantage, i.e. the converged solution, with sufficient accuracy, can be obtained if the flow condition $j_L < 0.3$ m/s is satisfied.

Figures 12(a, b) show the distributions of R_A^+ and R_D^+ obtained by using Dallman's (1978) correlation in Laurinat's method for the same cases as shown in figures 7(c, d). These distributions are characteristic in that the local liquid flow rate below which atomization does not occur is slightly larger than that determined by the present method.

Figures 13(a, b), which are similar to figures 10(a–h), show the circumferential distributions of each component relevant to the circumferential liquid flow rate, Γ_x. As clearly shown in these

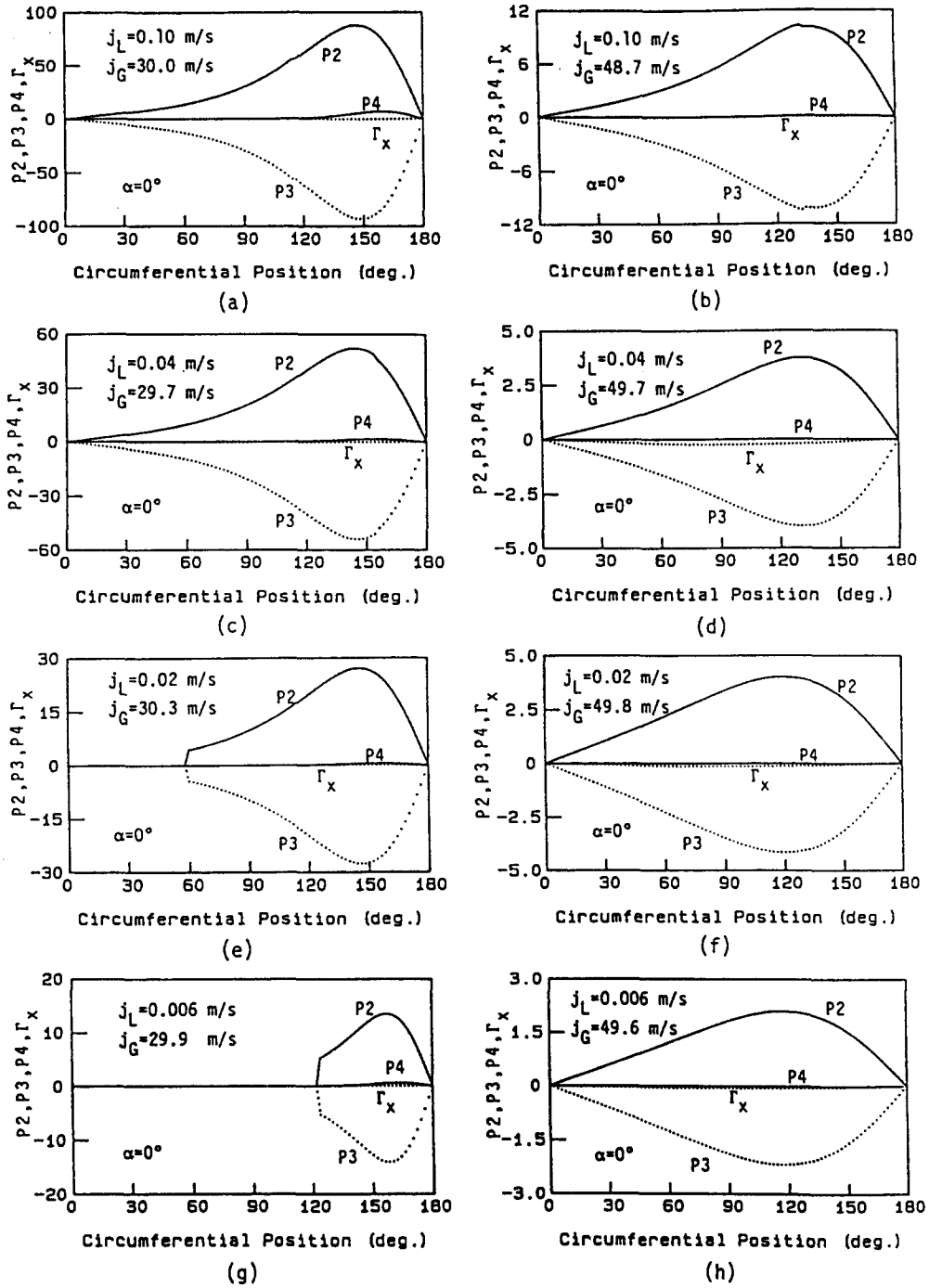

Figure 10. Distributions of the circumferential liquid flow rate predicted by the present method ($\alpha = 0°$).

figures, the dominating factor in controlling the film thickness distribution is the secondary gas flow, expressed by the first term on the l.h.s. of [12], P1, which is the most remarkable difference in comparison with the present theory.

4.3. Comment on the values of C_l in [16]

As described in the previous sections the distribution of the film thickness can be estimated for a wide range of flow conditions by the present flow model in which the secondary gas flow is totally neglected. What the present authors stress in this paper is, however, that the pumping action of the disturbance wave is only one of the important factors, including the secondary gas flow, which

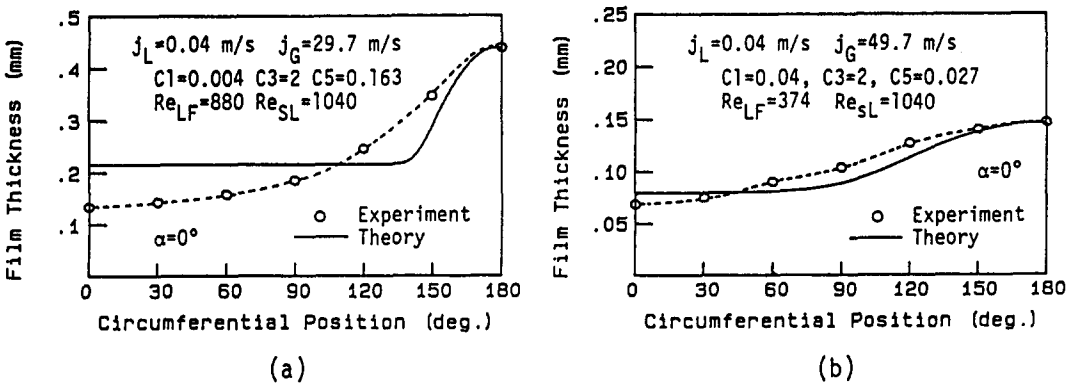

Figure 11. Distributions of the film thickness predicted by Laurinat's method ($\alpha = 0°$).

maintain the liquid film near the top of the pipe. That is, the value of C_1 is considered to be less than unity if the secondary gas flow has no effect on the film thickness distribution. As shown in figures 7(a–h) and 8(a–f), C_1 takes a value much larger than unity in some cases. The calculated result of the film thickness distribution is sensitive to the value of C_1, i.e. only a small change in C_1 decreases considerably the accuracy of the agreement between the calculated and the experimental data. Two possible reasons for this are (1) [16] may be not the best way to calculate ΔP and (2) the effect of the secondary gas flow may be included in the value of C_1. Therefore, the physical meaning of the magnitude of C_1 requires further investigation; modification and improvement of the present model is in progress.

5. CONCLUSIONS

A new flow model has been proposed to predict the circumferential distribution of the liquid film thickness in a horizontal and a near-horizontal annular flow, in which the disturbance waves transfer liquid towards the top of the tube mainly by a pumping action generated by the static pressure gradient along the disturbance wave. The predicted film thickness distributions were compared with the experimental data and those obtained with Laurinat's method. The results are summarized as follows:

(1) The pumping action of the disturbance wave is the most important factor in transferring liquid towards the top of the tube to cope with the drainage due to gravity for a wide range of flow conditions.
(2) The accuracy of the prediction of the circumferential film thickness distribution calculated by the present model is much better than that predicted by Laurinat's

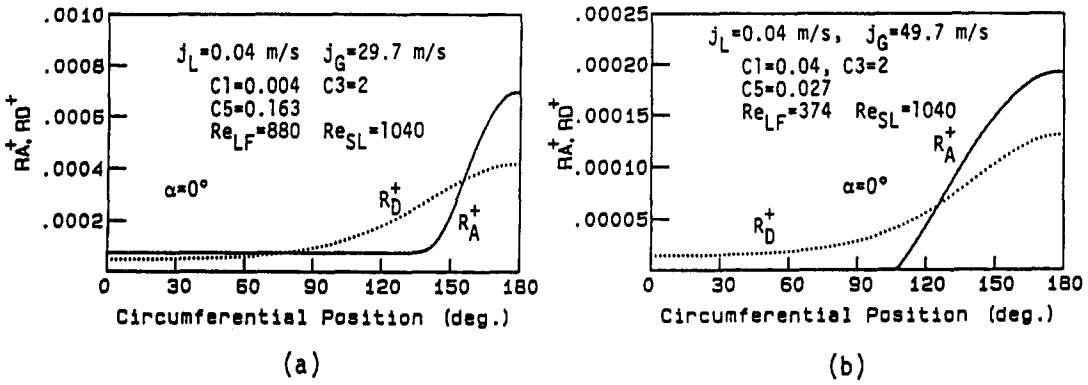

Figure 12. Distributions of the generation and deposition of entrainment predicted by Laurinat's method ($\alpha = 0°$).

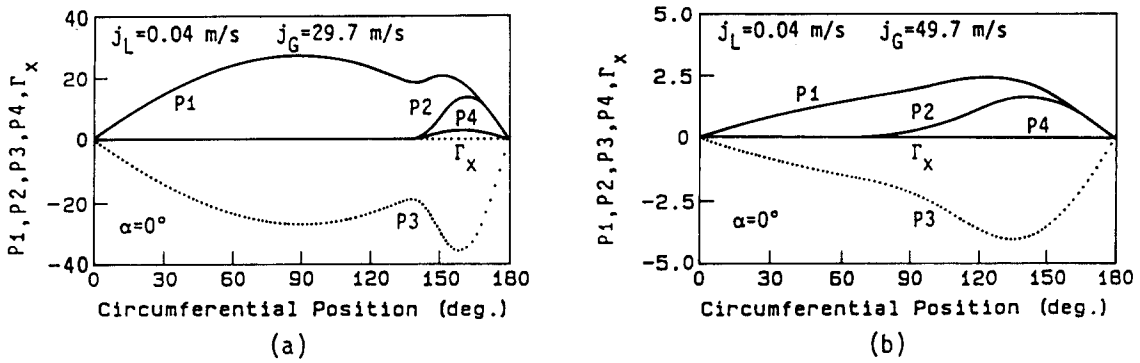

Figure 13. Distributions of the circumferential liquid flow rate predicted by Laurinat's method ($\alpha = 0°$).

model in the case where the liquid film covers the whole surface of the tube. The present method can be applied to a wider range of flow rates for both phases, including flow conditions where the solution cannot be obtained by Laurinat's model and where the liquid film breaks up near the top of the pipe, and also to flows in near horizontal pipes.

(3) In Laurinat's model there are two unknown constants in the basic equations with no direction given as to how to determine their values; in the present model there is only one and it is determined by the iteration method.

REFERENCES

BUTTERWORTH, D. 1973 An analysis of film flow for horizontal flow and condensation in a horizontal tube. Report AERE-R7575, pp. 1–18.

DALLMAN, J. C. 1978 Investigation of separated flow model in annular gas–liquid two-phase flows. Ph.D. Thesis, Univ. Illinois, Urbana.

FUKANO, T. & OUSAKA, A. 1987 Hold-up, frictional pressure drop and circumferential film thickness distribution of air–water two-phase annular flow in horizontal and near horizontal tubes. *Proc. 1987 ASME–JSME therm. Engng Joint Conf.* **5,** 359–366.

FUKANO, T., OUSAKA, A., MORIMOTO, T. & SEKOGUCHI, K. 1983 Air–water annular two-phase flow in a horizontal tube (Part 2, Circumferential variations of film thickness parameters). *Bull. Jap. Soc. mech. Engrs* **26,** 1387–1395.

FUKANO, T., OUSAKA, A., MORIMOTO, T. & SEKOGUCHI, K. 1985 Configuration of air–water two-phase annular flow in horizontal and near horizontal tubes. *Trans. Jap. Soc. mech. Engrs* **51,** 1807–1815. In Japanese.

FUKANO, T., ITOH, A., ODAWARA, H., KURIWAKI, T. & TAKAMATSU, Y. 1986 Liquid films flowing concurrently with air in horizontal duct (Part 5, Interfacial shear stress). *Bull. Jap. Soc. mech. Engrs* **28,** 2294–2301.

FUKANO, T., TOMINAGA, A., SAKAMOTO, T. & KATOH, E. 1987 Experimental study on the flow mechanism of a thin liquid film flowing concurrently with a high speed gas flow in a horizontal rectangular duct. *Proc. 1987 ASME–JSME therm. Engng Joint Conf.* **5,** 351–357.

HUTCHINSON, P. & WHALLEY, P. B. 1973 A possible characterisation of entrainment in annular flow. *Chem. Engng Sci.* **28,** 974–975.

LAURINAT, J. E., HANRATTY, T. J. & JEPSON, W. P. 1985 Film thickness distribution for gas–liquid annular flow in a horizontal pipes. *PhysicoChem. Hydrodynam.* **6,** 179–195.

LIN, T. F., JONES, O. C., LAHEY, R. T., BLOCK, R. C. & MURASE, M. 1985 Film thickness measurements and modeling in horizontal annular flows. *PhysicoChem. Hydrodynam.* **6,** 197–206.

OUSAKA, A., MORIMOTO, T. & MATUBARA, T. 1982 On the distribution of entrainment flow rate for air–water annular two-phase flow in a horizontal tube. *Scient. Pap. Fac. Engng Univ. Tokushima* **30,** 111–120. In Japanese.

SEKOGUCHI, K., FUKUI, H., MATSUOKA, T. & NISHIKAWA, K. 1975 Investigation into the statistical characteristics of bubble in two-phase flow (Part 1, Fundamentals of the investigation using the electric resistivity probe technique). *Bull. Jap. Soc. mech. Engrs* **18,** 391–396.

SEKOGUCHI, K., OUSAKA, A., FUKANO, T. & MORIMOTO, T. 1982 Air–water annular two-phase flow in a horizontal tube (Part 1, Circumferential distribution of film thicknesses). *Bull. Jap. Soc. mech. Engrs* **25,** 1559–1566.

WHALLEY, P. B., HEWITT, G. F. & HUTCHINSON, P. 1974 Experimental wave and entrainment measurements in vertical annular two-phase flow. *Chem. Engng Symp. Ser.*; No. 38, *Multiphase Flow Systems.*

WOODMANSEE, D. F. & HANRATTY, T. J. 1969 Mechanism for the removal of droplets from a liquid surface by a parallel air flow. *Chem. Engng Sci.* **24,** 299–307.